



Research

Micro and Nano Manipulation and Characterization—Article

Dynamic Deformation Measurement of an Intact Single Cell via Microfluidic Chip with Integrated Liquid Exchange



Xu Du ^a, Di Chang ^b, Shingo Kaneko ^b, Hisataka Maruyama ^a, Hiroataka Sugiura ^b, Masaru Tsujii ^c, Nobuyuki Uozumi ^c, Fumihito Arai ^{a,b,*}

^a Department of Micro-Nano Mechanical Science and Engineering, Nagoya University, Nagoya 464-8603, Japan

^b Department of Mechanical Engineering, The University of Tokyo, Tokyo 113-8656, Japan

^c Department of Biomolecular Engineering, Graduate School of Engineering, Tohoku University, Sendai 980-8579, Japan

ARTICLE INFO

Article history:

Received 28 July 2021

Revised 9 June 2022

Accepted 30 August 2022

Available online 15 February 2023

Keywords:

Microfluidic chip

Mechanical properties

Dynamic deformation

Single cell

Liquid exchange

ABSTRACT

This paper reports a method to measure the mechanical properties of a single cell using a microfluidic chip with integrated force sensing and a liquid exchange function. A single cell is manipulated and positioned between a pushing probe and a force sensor probe using optical tweezers. These two on-chip probes were designed to capture and deform the cells. The single cell is deformed by moving the pushing probe, which is driven by an external force. The liquid–liquid interface is formed between the probes by laminar flow to change the extracellular environment. The position of the interface is shifted by controlling the injection pressure. Two positive pressures and one negative pressure are adjusted to balance the diffusion and perturbation of the flow. The mechanical properties of a single *Synechocystis* sp. strain PCC 6803 were measured in different osmotic concentration environments in the microfluidic chip. The liquid exchange was achieved in approximately 0.3–0.7 s, and the dynamic deformation of a single cell was revealed simultaneously. Measurements of two Young's modulus values under alterable osmotic concentrations and the dynamic response of a single cell in osmotic shock can be collected within 30 s. Dynamic deformations of wild-type (WT) and mutant *Synechocystis* cells were investigated to reveal the functional mechanism of mechanosensitive (MS) channels. This system provides a novel method for monitoring the real-time mechanical dynamics of a single intact cell in response to rapid external osmotic changes; thus, it opens up novel opportunities for characterizing the accurate physiological function of MS channels in cells.

© 2023 THE AUTHORS. Published by Elsevier LTD on behalf of Chinese Academy of Engineering and Higher Education Press Limited Company. This is an open access article under the CC BY-NC-ND license (<http://creativecommons.org/licenses/by-nc-nd/4.0/>).

1. Introduction

The mechanical properties of cells are unique and important indexes that can be used to evaluate cells' biophysical properties. For example, it has been reported that mechanical forces play an important role in the formation, stabilization, and dissociation of focal adhesions and adherens junctions [1]. Other examples include the deformability of red blood cells, which decreases with stored time [2], and the stiffness of cancer cells, which is macroscopically lower than that of normal cells [3,4]. In addition, the mechanical properties of cells are critical factors in cellular division, migration, and growth [5,6].

The mechanical properties of cells can be measured with conventional methods such as atomic force microscopy (AFM) [7–

10], microplate manipulation [11,12], micropipette aspiration [13,14], and optical tweezers [2,15]. AFM has high sensitivity and resolution. However, it requires fixing the cells to a substrate, which is not easily done for suspended cells in general [16]. In some methods, the accuracy of microplate manipulation and micropipette aspiration is lower, which is unsuitable for the measurement of cells within a few micrometers. Moreover, the probe or pipette must be set in a three-dimensional (3D) space, which makes it difficult to capture images with a microscope [17]. Optical tweezers are suitable for manipulating single cells with a piconewton-order force, but the applied force is too weak to deform certain cells [16].

Robot-integrated microfluidic chips are a promising tool for characterizing the mechanical properties of a single cell. Confinement of the target cell's position in microchannels and the integration of a series of functional components on the chip enable high throughput and highly accurate manipulations and

* Corresponding author.

E-mail address: arai-fumihito@g.ecc.u-tokyo.ac.jp (F. Arai).

measurements [18,19]. Our previous papers describe the use of a series of microfluidic chips to measure the mechanical properties of cells individually and continuously [16,17,20,21]. Two on-chip probes were designed to capture and deform the cells. The pushing probe was moved by a piezo-actuator, and the reaction force was simultaneously measured using an on-chip force sensor probe composed of a hollow folded beam. To explore cellular characteristics in detail, we use phase detection of the moiré fringe to improve the measurement accuracy of movement of the probes.

Recently, we evaluated the response of mechanosensitive (MS) channels to changes in osmotic concentration. The mechanical properties of a model cyanobacterium, *Synechocystis* sp. strain PCC6803 (hereafter called *Synechocystis*), were measured via a robot-integrated microfluidic chip [16]. The diameter of a *Synechocystis* cell is approximately 2 μm , which is generally too small to manipulate. Members of the MS channel family in bacteria, including *Synechocystis*, can sense the cell membrane tension and release excess cytoplasmic solutes into the extracellular environment to protect the cell from a decrease in the extracellular osmotic concentration (i.e., osmotic down shock) [22,23]. Among the several MS channels in a *Synechocystis* cell, a large-conductance MS channel homolog (Mscl)—the plasma membrane-located Mscl (slr0875), plays a crucial role in cell volume recovery after osmotic down shock [23]. In 2018, we designed an opened chip to prevent the disturbance caused by bubbles in the microfluidic channel and altered the extracellular environment using a pipette [16]. This approach, which helps decrease the disturbance of the extracellular environment, enabled us to stably measure the mechanical property of a single cell. However, we could only measure the deformation of a single cell after an osmotic concentration change. Therefore, we could not measure cell deformation dynamically. In addition, an opened chip exposes cells to the external environment (and thus to the risk of contamination), and high throughput is not easily implemented.

In this paper, we propose a closed microfluidic chip integrated with a liquid exchange function. A liquid–liquid interface forms in the measurement area by laminar flow and is moved by controlling the injection pressure of the solutions. The pressure around the measurement area is adjusted by two positive pressures and one negative pressure to reduce flow perturbations. Based on this method, we measured the mechanical properties of single *Synechocystis* cells in environments with different osmotic concentrations. Furthermore, we analyzed the difference in the dynamic deformation processes of wild-type (WT) and mutant *Synechocystis* cells. Compared with the methods reported in previous research, this microfluidic chip can achieve a faster liquid exchange with low turbulence and can measure the dynamic deformation process and Young's modulus of a single cell within 30 s.

2. Material and methods

2.1. Overview of the on-chip cellular measurement system

The cell manipulation and measurement system consists of three parts (Fig. 1). The mechanical control part includes the jig, piezo-actuator, and probes in the robot-integrated microfluidic chip. Two on-chip probes were designed to capture and deform cells. The pushing probe is driven by a piezo-actuator, and the reaction force is simultaneously measured using a force sensor probe composed of a hollow folded beam. A displacement measurement method, called the sampling moiré method, is applied to enhance the sensing accuracy [17]. Small holes are patterned on the tips of the two probes and on the edge close to the measurement area. These small holes are used to generate moiré fringes that contribute to amplifying the displacement of the two probes, prevent-

ing the background noise of the image data from affecting the measurement.

The cell observation and manipulation part of the system includes optical tweezers, a microscope, and two charge-coupled-device (CCD) cameras. A single target cell in a microchannel is trapped at the focal point of the laser and transported by controlling the position of the focal point. Two high-speed cameras are integrated with this system to accurately measure the displacement of the two probes and the liquid–liquid interface, respectively. One monochrome camera with a wide field of view is used for measuring the displacement of the probes; the other red–green–blue (RGB) camera, with a high frame rate, is used to capture the distance moved by the liquid–liquid interface surrounding the cell.

The fluid control part of the system includes a microfluidic flow control system (MFCS-FLEX; Fluigent Corporation, France), syringe pump (KDS120; KD Scientific Inc., USA), and chip microchannels. There are three inlets in the microfluidic chip; two are used to inject solutions with different osmotic concentrations, and one is a spare microchannel (Fig. 1(b)). The microfluidic flow control system is connected to three inlets, which are used to apply positive pressure. The syringe pump is connected to an outlet and used to apply negative pressure to balance the pressure around the measurement area.

The fabrication process of the microfluidic chip is based on micro-electromechanical systems (MEMS) technology (supplementary information in Appendix A).

2.2. Cell culture and preparation

All the *Synechocystis* cells used in this study were provided by Tohoku University. Since the intracellular pressure of a *Synechocystis* cell is adjusted by MS channels when the osmotic concentration decreases, *Synechocystis* WT and Mscl-defective mutant (Δmscl) cells were used. The mutant cells had the insertion of a spectinomycin resistance gene in *symscL* gene (one gene encoding a putative large conductance mechanosensitive channel homolog, slr0875) [23]. Both cell types were cultured in a BG11 medium at a temperature of 28 °C for 6–7 days under continuous illumination (3.5 W light emitting diode (LED) white-light source). BG11 mixed with 0.5 $\text{mol}\cdot\text{L}^{-1}$ sorbitol was used as a low osmotic concentration (LOC) solution, and BG11 mixed with 1 $\text{mol}\cdot\text{L}^{-1}$ sorbitol was used as a high osmotic concentration (HOC) solution [23]. Prior to the experiment, the cells cultured in BG11 were centrifuged at 620g (g is gravitational acceleration) for 2 min and resuspended in HOC solution. A small amount of rhodamine B was introduced into the LOC solution to distinguish between the two solutions and make it possible to observe the liquid–liquid interface clearly. In addition, we mixed the green fluorescent dye SYTO 9 and the red fluorescent dye propidium iodide (PI) into the solutions, as these dyes make it possible to remove dead or damaged cells before an experiment (supplementary information).

2.3. Compression model and force sensor calibration

The compression concept is shown in Fig. 2(a). A single cell or bead is squeezed by driving a piezo-actuator to move the pushing probe. The sensor probe is connected to a folded beam force sensor, which can transduce the displacement to force (Fig. 2(b)). Hence, the deformation and stress of the target object can be estimated by measuring the movement of the two probes. When the pushing probe is driven, the point where the sensor probe has a displacement is defined as the deformation start position. We then successively drive the pushing probe to squeeze the cell and the

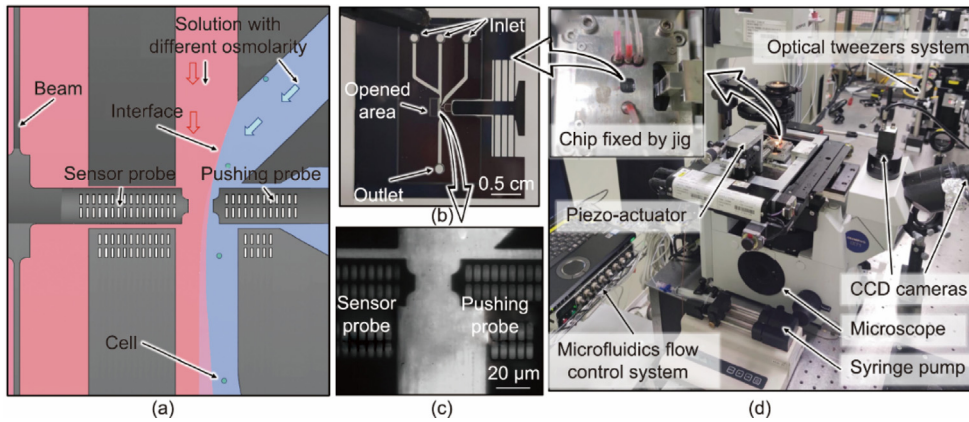


Fig. 1. Overview of the experimental setup and the microfluidic chip. (a) Conceptual diagram of the measurement area at the microfluidic chip; (b) fabricated robot-integrated microfluidic chip; (c) microscopic image of the measurement area; (d) photograph of the experimental setup. CCD: charge-coupled-device.

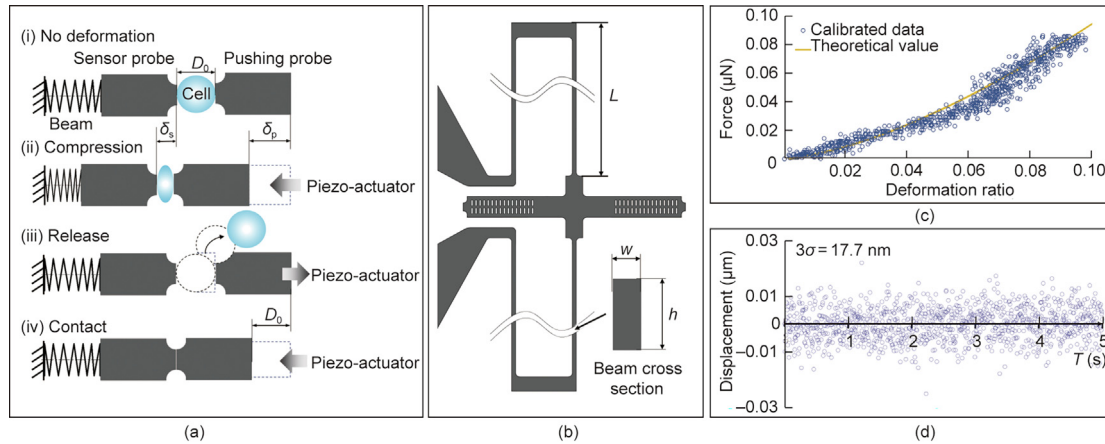


Fig. 2. The compression concept, force sensor design, and calibration. (a) Concept of the measurement process; (b) design of the force sensor part; (c) an example of the theoretical value and calibration data of the force sensor (dark blue dots show data measured using the microfluidic chip after calibration; the orange curve shows the theoretical values when the Young’s modulus of polydimethylsiloxane (PDMS) is 0.98 MPa); (d) stability of displacement of the sensor probe. D_0 : the original diameter of the cell; δ_s , δ_p : the displacement of the sensor probe and the pushing probe, respectively; L , w , h : the length, width, and thickness of the rectangular beam, respectively; σ : standard deviation (SD); T : time.

sensor probe. The sensor probe and the pushing probe have displacements of δ_s and δ_p , respectively.

The deformation of the cell, δ_c , can be calculated by the difference in the displacement of two probes:

$$\delta_c = \delta_p - \delta_s \quad (1)$$

To measure the original diameter of the target object, the pushing probe is driven to touch the tip of the sensor probe, and the difference in the displacement with and without the cell is taken as the original diameter of the cell, D_0 .

Hence, the diameter of the cell, D_c , can be represented by the following equation:

$$D_c = D_0 - \delta_c \quad (2)$$

The Hertzian model can be used to describe the relationship between the deformation of a sphere and the force for non-adhesive elastic contact [24,25]. This model is widely used for measuring the Young’s modulus of cells with a small deformation [26,27]. The equation can be simplified as follows:

$$F = k\delta_s = \frac{4(D_0/2)^{1/2}}{3} \cdot \frac{E_c}{1-\nu^2} \cdot \left(\frac{\delta_c}{2}\right)^{3/2} \quad (3)$$

where F represents the reaction force (N); k is the spring constant of the force sensor ($\text{N}\cdot\text{m}^{-1}$); E_c is the Young’s modulus of the cell (Pa), and ν is the Poisson’s ratio of the cell. The Poisson’s ratio is taken to be 0.5 by assuming that the cell is composed of incompressible materials.

The spring constant of an end-loaded thin beam with a rectangular cross-section can be estimated by the following equation [28]:

$$k = w^3 h E_b / L^3 \quad (4)$$

where E_b is the Young’s modulus of the beam (Pa); L , w , and h represent the length, width, and thickness of the rectangular beam, respectively (m). In this study, Eq. (4) is used to evaluate the spring constant of the force sensor beam.

The spring constant of the force sensor beam in the microfluidic chip was calibrated using polydimethylsiloxane (PDMS) beads. The specific production process has been reported in our previous work [16]. The PDMS beads and PDMS bars were fabricated under the same conditions. Hence, the Young’s moduli of the beads and bars are similar values. The Young’s modulus of the PDMS bar was approximately 0.98 MPa, as measured by a load sensor (LVS-10GA; Kyowa Electronic Instruments Co., Ltd., Japan). The PDMS beads were then measured to calibrate the spring constant of the

force sensor (Fig. 2(c)). The average calibrated spring constant (mean (standard deviation (SD))) was 0.0488 (0.0160) N·m⁻¹.

We calculate the reaction force by measuring the displacement of the sensor probe. Therefore, the resolution of the force measurement depends on the resolution of the displacement measurement. We used the sampling moiré method to enhance the resolution of the displacement measurement [17]. The principle of the sampling moiré method is described below. First, grating patterns with a constant period are etched on the tips of two probes (Fig. 1(c)). A grayscale image of the two probes is obtained by using the assembled CCD camera of the microscope. Next, a down sampling process is applied for every few pixels of the image, and the moiré fringe can be exposed by means of an interpolation process. Fourier transformation is used to analyze the intensity of the moiré fringe. Hence, the displacement of the probe is determined by measuring the phase shift of the moiré fringe [16,17]. The measurement noise for the displacement of the sensor probe in the experimental environment was recorded for 5 s to verify the accuracy of the microfluidic chip (Fig. 2(d)). The stability of the displacement achieved by 3σ is 17.7 nm (where σ is the SD), which corresponded to a force resolution of 0.864 nN.

2.4. Control of the liquid exchange

An important process in cell measurement is changing the extracellular environment to simultaneously expose cells to stimulation and detection. With laminar flow, the liquid environment surrounding the cells can be exchanged quickly and simply [29]. Flow switching using laminar flow is often used in cell sorting, labeling, and analysis [30–34]. However, it is difficult to use laminar flow in force measurements, since the pressure variation in laminar flow control will disturb the force sensor. To accurately measure the dynamic characteristics of cells, the effects of the liquid exchange should be reduced as much as possible. Decreasing the flow velocity and the pressure required for the liquid exchange can reduce these effects. However, the time required for the liquid exchange and the amount of diffusion in the laminar flow will be increased. It is important to ensure that the measured cell is completely separated from the initial solution and immersed in the exchanged reagent.

The liquid exchange process is shown in Fig. 3. In Fig. 3(a), pressure is applied to remove bubbles in the microchannels and to ver-

ify that a stable liquid–liquid interface is present in the main microchannel. Subsequently, the pressure of the LOC solution is removed to cause the measurement area to be covered by the HOC solution. Hence, the cells in the microchannel are immersed in the HOC environment. In Fig. 3(c), all pressure sources are closed to reduce the flow speed. The cell is trapped by optical tweezers and moved to the area between the two probes. After trapping the cell, the cell is pinched by driving the piezo-actuator. The pinch force must be carefully controlled to prevent large deformations. Otherwise, the Young’s modulus measured in the HOC condition will not be reliable. In fact, the extracellular polysaccharides of *Synechocystis* are soft and sticky, so it is possible to slightly compress the cell by moving the pushing probe, and then release the pushing probe after a few seconds. The cell will adhere to the tip of the probe, which prevents it from being washed away by the stream. Alternatively, it is possible to control the two probes with an appropriate distance and place the cell upstream of the probes using optical tweezers. When the pressure of the HOC solution is slightly increased to detach the cell from the optical tweezers, the cell will flow between the probes. Because the extracellular polysaccharides are soft, the flowing cell will be captured by the two probes, and the deformation of the polysaccharides will not change the stiffness of the cell.

After the flow speed becomes stable, the recording (t_0) is started. In Fig. 3(d), the target cell is squeezed by driving the piezo-actuator, and the Young’s modulus of a single cell in the HOC condition can be measured. Subsequently, the pressure of the HOC solution is gradually increased, and the pressure of the LOC solution is slightly increased to maintain the interface on the left side of the cell; this keeps the cell immersed in the HOC condition. After trapping and measuring the cell in the HOC condition, the injection pressure of the LOC solution is rapidly increased (t_1) to exchange the solutions. In this step, the dynamic deformation of the target cell and the process of liquid exchange can be recorded by high-speed cameras. After a few seconds, the pushing probe is released by the actuator (t_2); then, the Young’s modulus of the cell in the LOC condition is measured, as shown in Fig. 3(e).

We performed a series of experiments to determine the appropriate pressure range with low perturbation. Solutions with the same osmotic concentration were injected into both microchannels to remove the effect of osmotic shock and expose the disturbance caused by the liquid exchange (Fig. 4(a)).

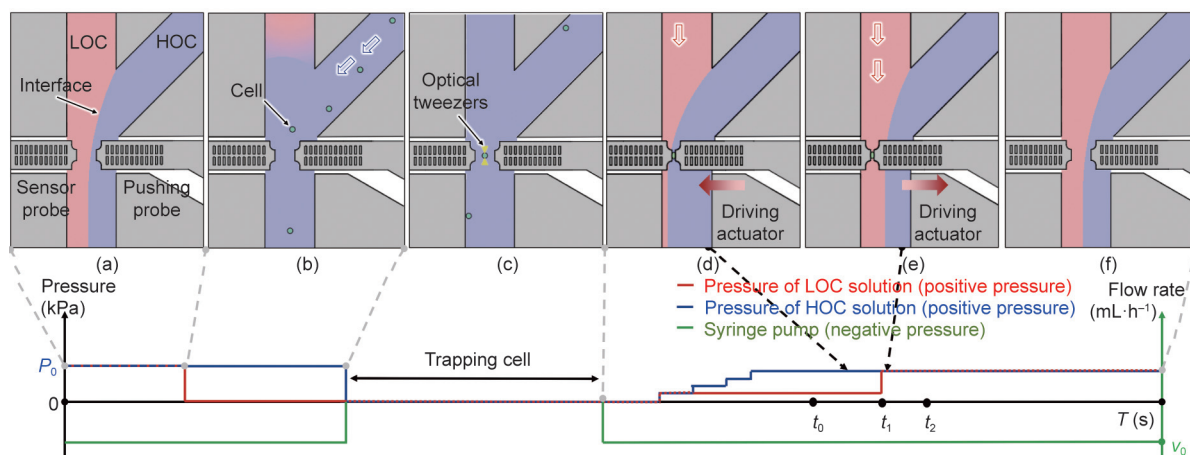


Fig. 3. The cell manipulation and liquid exchange process, with the curves underneath showing the pressure corresponding to each step. (a) Pressure is applied to remove bubbles in the microchannels and verify that a stable liquid–liquid interface is present in the middle of the main microchannel; (b) the cells in the microchannel are immersed in HOC solution; (c) the single cell is manipulated by optical tweezers and probes; (d) the target cell is compressed, and the Young’s modulus of the cell is measured in the HOC; (e) the Young’s modulus of the target cell is measured in the LOC; (f) the cell is released. t_0 : the start of the recording; t_1 : the time at which the solutions are exchanged; t_2 : the time at which the pushing probe is released; P_0 : the initial pressure applied by the microfluidics flow control system; v_0 : the initial flow speed applied by the syringe pump.

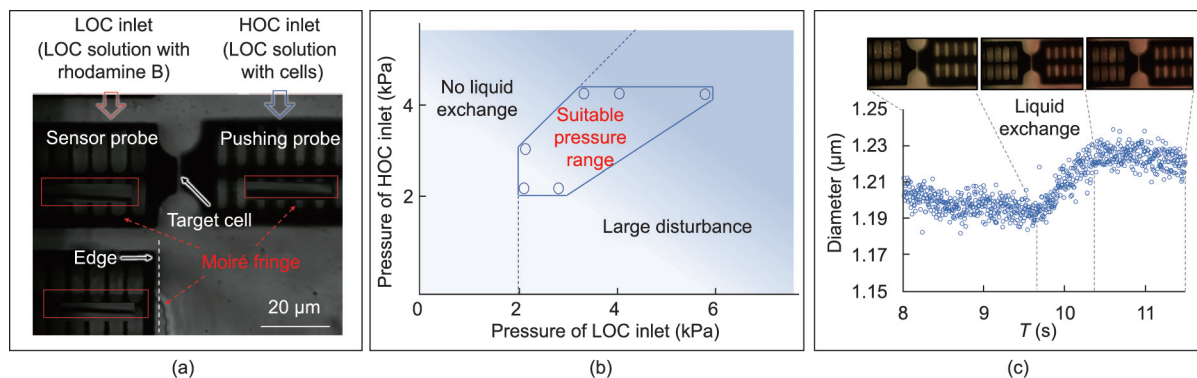


Fig. 4. Pressure control and liquid exchange in the microfluidic chip. (a) Microscopic image of the measurement area. In the perturbation test, both microchannels were injected with the LOC solution. (b) The pressure range for a small disturbance is shown with a blue outline, and the blue dots are data used to determine the boundary of the range. (c) The curve represents the dynamic deformation of the cell during the perturbation measurement (blue dots), and the figures above the curve show the measurement area.

When the liquid exchange was performed, the pressure of the LOC increased sharply to shift the interface from the left side to the right side of the cell. However, when the injection pressure of the LOC was too low to pass the interface through the cell, liquid exchange was not achieved (for no liquid exchange, see Fig. 4(b)). When the pressure of the LOC is much greater than the other pressure or is greater than 6 kPa, the sharply increased pressure applies a huge impact on the sensor probe. The dynamic response of the cell deformation collected in such a case is not reliable. Therefore, the suitable pressure is limited to a small range.

An example of the perturbation test is shown in Fig. 4(c). The curve represents the dynamic deformation of the cell, and the figures above the curve show microscopic images of the measurement area. The liquid–liquid interface can be seen in the second image; the curve corresponding to this image shows the perturbation when the liquid exchange was performed, which was approximately 30 nm. Given that there was no osmotic change during this process, the diameter change (i.e., the deformation) should be caused by the disturbance of the liquid exchange. This perturbation is small enough (which will be explained in Section 3), so this experimental condition is used in the later experiments.

In the experiments, we used a syringe pump to control the flow speed of the main microchannel at approximately $0.1 \text{ mL}\cdot\text{h}^{-1}$ ($20\text{--}30 \text{ mm}\cdot\text{s}^{-1}$ in the measurement area). The injection pressure of the HOC inlet was 4 kPa. When the injection pressure of the LOC inlet was increased (from 0–1 to 4 kPa) to exchange the solutions, the interface shifted by approximately $40 \mu\text{m}$. To ensure that the measured cell was completely immersed in the exchanged solution, the movement distance of the interface was made to be larger than the range of diffusion (i.e., diffusion distance). We measured the diffusion distance by analyzing the grayscale level around the position of the interface. It was approximately $5.3 \mu\text{m}$ (supplementary information). The movement distance of the interface was far larger than the diffusion distance; hence, the extracellular solution was completely replaced. The following experiments were conducted under these conditions.

In addition to controlling the pressures, we reduced the disturbance of the liquid exchange by means of the structural designs of the microfluidic chip (supplementary information).

3. Results

When driving the pushing probe to squeeze the cell, the maximum compression force was stable at approximately $0.2 \mu\text{N}$, which deformed the cell by 20%–30%. We calculated the Young's modulus of the cell using the Hertzian model (Eq. (3)). Only 10% deforma-

tion was used to calculate the Young's modulus of the cell, because the Hertzian model is only reliable for a small deformation of an elastic sphere. Although a cell is not a perfectly elastic body, cells always have very complex mechanical properties, such as viscoelasticity, poroelasticity, and plasticity [35,36]. We have observed that cells cannot recover from deformation after a long period of compression. However, in our previous work, we demonstrated the feasibility of using the Hertzian model to calculate the Young's modulus of *Synechocystis* with a small deformation [16]. A study has also reported that there is no major difference between the fitting curves using viscoelastic and poroelastic models [37]. In this experiment, the compression of a single cell took several seconds, and the damping effect of the viscoelasticity could be ignored. The maximum compression force duration (i.e., the time of the liquid exchange process) was limited to less than 5 s to prevent a change in the Young's modulus because of compression for a long duration (Fig. 5). The time points t_1 and t_2 in Fig. 3 are determined under these conditions.

The two curves in Fig. 5(b) represent the displacements of the pushing and sensor probes, while the increasing direction of the vertical axis represents the displacement to the right (i.e., the direction of the pushing probe). For the first 7 s, we drove the pushing probe to squeeze the cell. As mentioned above, a cell deformation of 10% was used to calculate the Young's modulus. Hence, the data at approximately 0–5 s of Fig. 5(b) can be converted to Fig. 5(c) (blue coverage area on the left). The Young's modulus of the cell in the HOC environment can be evaluated by the fitting curve in Fig. 5(c).

The deformation ratio δ_c/D_0 at the horizontal axis label of Figs. 5(c) and (e) represent the ratio of the amount of deformation to the original diameter D_0 . From $T = 7 \text{ s}$ to 11 s , the pushing probe was stopped, and the solution environment around the cell was alternated from HOC to LOC at t_1 . The dynamic deformation of a single cell can be observed in these 4 s. The curve in Fig. 5(d) shows that the squeezed *Synechocystis* cell swells during the liquid exchange and shrinks slightly after the liquid exchange—a finding that is unreported in any research. In addition, the peak of the cell deformation before and after the osmotic down shock is approximately 15% ($0.33 \mu\text{m}$). However, as shown in Section 2.4, the peak of the perturbation before and after the liquid exchange is approximately 30 nm under the same experimental conditions, which is far smaller than that of the cell deformation during the osmotic shock. Hence, the realized low-disturbance liquid exchange system is feasible for cell deformation measurement.

The cell size ratio D_c/D_0 at the vertical axis label of Fig. 5(d) represents the ratio of the cell diameter after deformation to the original diameter. After the liquid exchange, the pushing probe was

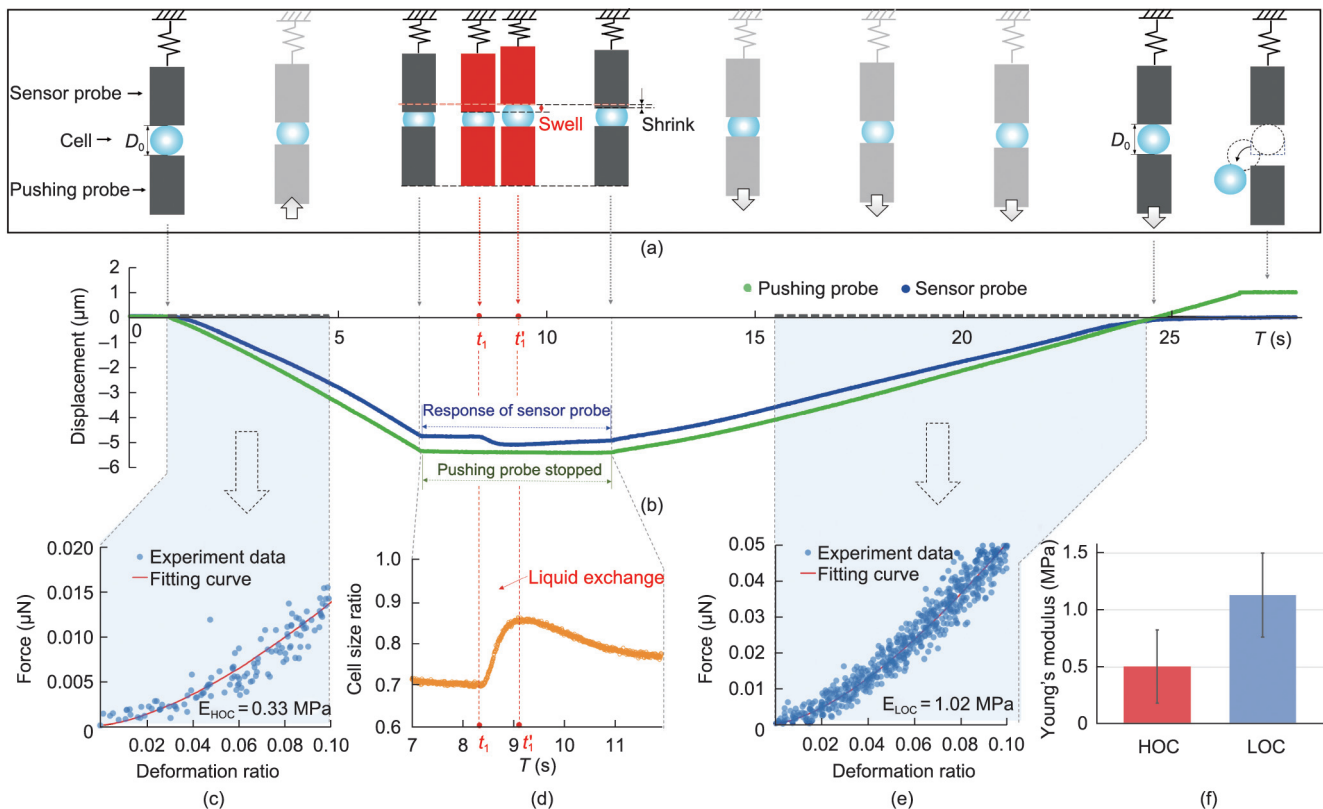


Fig. 5. An example of the measurement result for WT *Synechocystis*. (a) Schematic of the position of the two probes and the deformation of a single cell. (b) The blue dots show the displacement of the sensor probe, and the green dots show the displacement of the pushing probe. (c) Force–deformation ratio for the HOC. Blue dots show the experimental data and the red line shows the fitted Hertzian model. (d) Dynamic deformation (cell size change) ratio with respect to the time of a single cell during the liquid exchange. (e) Force–deformation ratio for the LOC. Blue dots show the experimental data, and the red line shows the fitted Hertzian model. (f) The red bar represents the average Young's modulus (mean (SD)) in the HOC solution (0.51 (0.32) MPa), and the blue bar represents the average Young's modulus (mean (SD)) in the LOC solution (1.13 (0.37) MPa). t_1 : the time at which the extracellular environment is exchanged; E_{HOC} : the Young's modulus of a single cell in the HOC solution; E_{LOC} : the Young's modulus of a single cell in the LOC solution.

released; the data in approximately 15–25 s of Fig. 5(b) can be converted to Fig. 5(e) (blue coverage area on the right). The Young's modulus in the LOC environment was calculated in this step. Notably, the disturbance of the liquid exchange happened when the pushing probe was stopped (at approximately 7–11 s in Fig. 5(b)), which is revealed by the data used to calculate the Young's modulus (at approximately 0–5 and 15–25 s; the blue coverage area in Fig. 5(b)). Therefore, the disturbance does not affect the calculation accuracy of the Young's modulus. In short, this study can measure the two Young's moduli of the same cell under different osmotic concentrations, as well as the dynamic response of a single cell in osmotic shock within 30 s.

The average value of the Young's modulus (mean (SD)) in the LOC solution was 1.13 (0.37) MPa (95% confidence interval (CI), 0.96–1.30), and the average value of the Young's modulus (mean (SD)) in the HOC solution was 0.51 (0.32) MPa (95% CI, 0.35–0.65) (Fig. 5(f)). Twenty cells were measured in each bar. Compared with the results from our previous research, the values of the Young's modulus in the HOC solution (BG11 mixed with 1 mol·L⁻¹ sorbitol) were very close, and the value of the Young's modulus in LOC (BG11 mixed with 0.5 mol·L⁻¹ sorbitol) was larger than that in HOC and smaller than that in pure BG11 solution [16]. These comparisons elucidated that the measurement results in this experiment were reliable.

To explore the function of MS channels in *Synechocystis* cells, we measured the dynamic deformation of WT and Δ mscL *Synechocystis* cells. Figs. 6(a) and (b) show examples of the dynamic deformation of a single WT cell and a single mutant cell during the liquid

exchange. As mentioned above, the cell size ratio D_t/D_0 in the vertical axis label of the figure represents the ratio of the cell diameter after deformation to the original diameter. The peak D_1 represents the maximum cell expansion ratio before and after the liquid exchange. D_2 represents the deformation ratio change 3 s after the liquid exchange started, and D_3 represents the decrease in the deformation ratio by shrinkage, which is also the difference between D_1 and D_2 . Because *Synechocystis* has a spherical cell shape without obvious polarity [38], the cell volume can be estimated as the volume of a sphere. As shown in Figs. 6(a) and (b), the difference in D_1 between the WT and Δ mscL cells was not significant. However, the cell volume of the WT cells decreased faster than that of the Δ mscL cells. This finding accounts well for the function of MscL when the cells were subjected to hypoosmotic shock. The statistical result for the apparent cell volume is shown in Fig. 6(c). The error bars in Figs. 6(c) and (d) show the SD. The apparent cell volume of the mutant cells (95% CI, 4.37–5.22) is slightly larger than that of the WT cells (95% CI, 3.75–5.41), which is consistent with the findings in previous research [39]. A comparison of three typical deformation values in the dynamic deformation curve between WT and Δ mscL is shown in Fig. 6(d). Over 10 cells were measured in each bar. The deformation ratio of D_1 and D_2 in WT are smaller than in Δ mscL, and the shrinkage value D_3 in WT is larger than that in Δ mscL. The 95% CI of the deformation ratio data is as follows: WT D_1 , 95% CI, 0.07–0.10; WT D_2 , 95% CI, -0.04–0.04; WT D_3 , 95% CI, 0.05–0.12; Δ mscL D_1 , 95% CI, 0.07–0.13; Δ mscL D_2 , 95% CI, 0.01–0.04; and Δ mscL D_3 , 95% CI, 0.04–0.11.

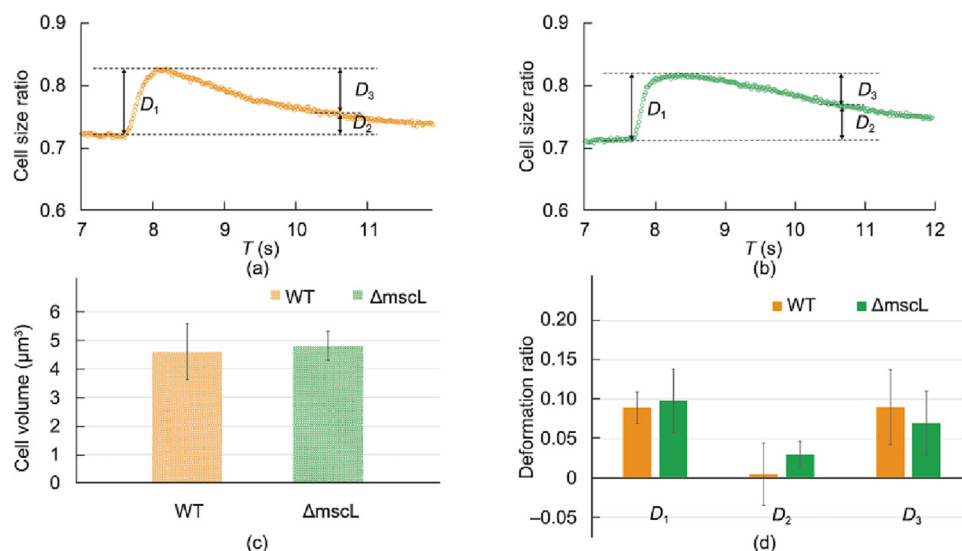


Fig. 6. Dynamic deformation (cell size change) of WT and Δ mscL *Synechocystis* cells. Examples of (a) the dynamic deformation of a single WT cell and (b) the dynamic deformation of a single mutant cell during the liquid exchange; (c) apparent cell volume of WT (orange) and mutant (green) cells; (d) comparison of D_1 , D_2 , and D_3 between WT (orange) and mutant (green) cells.

4. Discussion

A microfluidic chip with an integrated liquid exchange function was developed and was used to measure the dynamic deformation of a single *Synechocystis* cell. The cell exposed an intriguing deformation when liquid was exchanged (Fig. 5(d)). The deformation first reached a peak (i.e., the swelling of a single cell from t_1 to t'_1), where the time to the peak depended on the speed of the liquid exchange. The speed of the liquid exchange was approximately 0.3–0.7 s (the average value of the liquid exchange time (mean (SD)) in WT was 0.49 (0.09) s, and that in Δ mscL was 0.47 (0.15) s), which was fast enough to expose the dynamic deformation of the cell. The value of this peak (i.e., the cell deformation before and after the osmotic down shock) was approximately 0.3 μ m. The perturbation of the liquid exchange was approximately 0.03 μ m, which could be ignored in comparison with the value of the peak. After reaching the peak, the cell slightly shrank. A study has measured cell size or volume using a non-contact method and reported that *Synechocystis* will rapidly swell under osmotic down shock; subsequently, the size of the cell will remain unchanged [23].

To explain this phenomenon, we provide a hypothesis here: When the osmotic concentration decreases (i.e., osmotic down shock), water enters the cell and makes it swell; the MS channel then senses the increased membrane tension force and releases the intracellular components [40,41]. However, in our experiment, the cell was compressed, which increased the membrane tension force. After osmotic down shock, the MS channel still received a response indicating a high membrane tension force; hence, it continued to release the intracellular components, causing the cell to shrink. To prove this hypothesis, we compared the difference in the dynamic deformations of WT and mutant *Synechocystis* cells. The difference in the peak value D_1 was not apparent in the statistical result. However, the recovery of the Δ mscL cells to the original cell volume was slower than that of the WT cells (as indicated by the values of D_2 and D_3), since the Δ mscL cells could not release the intracellular components using MS channels to adapt to the osmotic down shock (Fig. 6). After the liquid exchange was completed, the WT cells showed obvious shrinkage compared with the Δ mscL cells, which proved that the MS channel can sense an external force and release cytoplasm to protect the cell from bursting.

5. Conclusions

In this work, we proposed a system that integrates the functions of cell manipulation, flow control, and cellular force measurement for evaluating the mechanical properties of a single cell. A robot-integrated microfluidic chip was fabricated using MEMS technology and combined with a liquid exchange function to alter osmotic concentrations. A liquid–liquid interface can be formed at the measurement area by laminar flow and can be shifted by adjusting the injection pressures. The low disturbance range of the injection pressures was revealed by an experiment without an osmotic concentration change. The Hertzian model was used to calculate the Young's modulus of *Synechocystis*. The deformation and reaction forces of one cell under different osmotic concentrations were measured. The average value of the Young's modulus in the LOC solution (BG11 mixed with 0.5 mol·L⁻¹ sorbitol) was (1.13 \pm 0.37) MPa, and the average value of the Young's modulus in the HOC solution (BG11 mixed with 1 mol·L⁻¹ sorbitol) was (0.51 \pm 0.32) MPa. Compared with our previous research, the Young's modulus values obtained in this study were reasonable. In addition, the dynamic deformation of a single *Synechocystis* cell was revealed in this study. The squeezed cell first swelled when the osmotic concentration decreased and then slightly shrank. Moreover, the dynamic deformation processes of WT and mutant *Synechocystis* were compared. These results confirm that MS channels work to release cytoplasm to adapt to the extracellular environment.

Acknowledgments

This work was partially supported by Grants-in-Aid for Scientific Research from the Ministry of Education, Culture, Sports, Science, and Technology (18H03762 and 21H04543 to Fumihito Arai and Nobuyuki Uozumi). We thank the Chinese Scholarship Council for supporting the author Du Xu in his PhD study.

Compliance with ethics guidelines

Xu Du, Di Chang, Shingo Kaneko, Hisataka Maruyama, Hiroataka Sugiura, Masaru Tsujii, Nobuyuki Uozumi, and Fumihito Arai declare that they have no conflict of interest or financial conflicts to disclose.

Appendix A. Supplementary data

Supplementary material to this article can be found online at <https://doi.org/10.1016/j.eng.2022.08.020>.

References

- [1] Chen CS, Tan J, Tien J. Mechanotransduction at cell–matrix and cell–cell contacts. *Annu Rev Biomed Eng* 2004;6:275–302.
- [2] Li Y, Wen C, Xie H, Ye A, Yin Y. Mechanical property analysis of stored red blood cell using optical tweezers. *Colloids Surf B Biointerfaces* 2009;70(2):169–73.
- [3] Miyanaga N, Akaza H, Yamakawa M, Oikawa T, Sekido N, Hinotsu S, et al. Tissue elasticity imaging for diagnosis of prostate cancer: a preliminary report. *Int J Urol* 2006;13(12):1514–8.
- [4] Beil M, Micoulet A, von Wichert G, Paschke S, Walther P, Omary MB, et al. Sphingosylphosphorylcholine regulates keratin network architecture and visco-elastic properties of human cancer cells. *Nat Cell Biol* 2003;5(9):803–11.
- [5] Lautenschläger F, Paschke S, Schinkinger S, Bruel A, Beil M, Guck J. The regulatory role of cell mechanics for migration of differentiating myeloid cells. *Proc Natl Acad Sci USA* 2009;106(37):15696–701.
- [6] Huang S, Ingber DE. The structural and mechanical complexity of cell-growth control. *Nat Cell Biol* 1999;1(5):E131–8.
- [7] Dufrene YF. Atomic force microscopy, a powerful tool in microbiology. *J Bacteriol* 2002;184(19):5205–13.
- [8] Sit PS, Kohn J. Cell membrane micromechanical properties on polymeric surfaces studied by atomic force microscopy. *Biophys J* 2003;84(2):296A.
- [9] Franz CM, Puech PH. Atomic force microscopy: a versatile tool for studying cell morphology, adhesion and mechanics. *Cell Mol Bioeng* 2008;1(4):289–300.
- [10] Chang D, Hirate T, Uehara C, Maruyama H, Uozumi N, Arai F. Evaluating Young's modulus of single yeast cells based on compression using an atomic force microscope with a flat tip. *Microsc Microanal* 2021;27(2):392–9.
- [11] Thoumine O, Ott A. Time scale dependent viscoelastic and contractile regimes in fibroblasts probed by microplate manipulation. *J Cell Sci* 1997;110(17):2109–16.
- [12] Thoumine O, Ott A, Cardoso O, Meister JJ. Microplates: a new tool for manipulation and mechanical perturbation of individual cells. *J Biochem Biophys Methods* 1999;39(1–2):47–62.
- [13] Hochmuth RM. Micropipette aspiration of living cells. *J Biomech* 2000;33(1):15–22.
- [14] Liu X, Wang Y, Sun Y. Real-time high-accuracy micropipette aspiration for characterizing mechanical properties of biological cells. In: *Proceedings of 2007 IEEE International Conference on Robotics and Automation*; 2007 Apr 10–14; Rome, Italy. IEEE; 2007. p. 1930–5.
- [15] Zheng XR, Zhang X. Microsystems for cellular force measurement: a review. *J Micromech Microeng* 2011;21(5):054003.
- [16] Chang D, Sakuma S, Kera K, Uozumi N, Arai F. Measurement of the mechanical properties of single *Synechocystis* sp. strain PCC6803 cells in different osmotic concentrations using a robot-integrated microfluidic chip. *Lab Chip* 2018;18(8):1241–9.
- [17] Sugiura H, Sakuma S, Kaneko M, Arai F. On-chip method to measure mechanical characteristics of a single cell by using moiré fringe. *Micromachines* 2015;6(6):660–73.
- [18] Koike Y, Yokoyama Y, Hayakawa T. Light-driven hydrogel microactuators for on-chip cell manipulations. *Front Mech Eng* 2020;6:1–9.
- [19] Takayama Y, Perret G, Kumemura M, Ataka M, Meignan S, Karsten SL, et al. Developing a MEMS device with built-in microfluidics for biophysical single cell characterization. *Micromachines* 2018;9(6):275.
- [20] Sakuma S, Arai F. Cellular force measurement using a nanometric-probe-integrated microfluidic chip with a displacement reduction mechanism. *J Robot Mechatron* 2013;25(2):277–84.
- [21] Nakahara K, Sakuma S, Hayakawa T, Arai F. On-chip transportation and measurement of mechanical characteristics of oocytes in an open environment. *Micromachines* 2015;6(5):648–59.
- [22] Ajouz B, Berrier C, Garrigues A, Besnard M, Ghazi A. Release of thioredoxin via the mechanosensitive channel MscL during osmotic downshock of *Escherichia coli* cells. *J Biol Chem* 1998;273(41):26670–4.
- [23] Nanatani K, Shijuku T, Akai M, Yukutake Y, Yasui M, Hamamoto S, et al. Characterization of the role of a mechanosensitive channel in osmotic down shock adaptation in *Synechocystis* sp PCC 6803. *Channels* 2013;7(4):238–42.
- [24] Hertz H. On the contact of elastic solids. *J Reine Angew Math* 1881;92:156–71.
- [25] Johnson KL. *Contact mechanics*. Cambridge: Cambridge University Press; 1987.
- [26] Kuznetsova TG, Starodubtseva MN, Yegorenkov NI, Chizhik SA, Zhdanov RI. Atomic force microscopy probing of cell elasticity. *Micron* 2007;38(8):824–33.
- [27] Rosenbluth MJ, Lam WA, Fletcher DA. Force microscopy of nonadherent cells: a comparison of leukemia cell deformability. *Biophys J* 2006;90(8):2994–3003.
- [28] Albrecht TR, Akamine S, Carver TE, Quate CF. Microfabrication of cantilever styli for the atomic force microscope. *J Vac Sci Technol A* 1990;8(4):3386–96.
- [29] Tarn MD, Lopez-Martinez MJ, Pamme N. On-chip processing of particles and cells via multilaminar flow streams. *Anal Bioanal Chem* 2014;406:139–61.
- [30] Ong SE, Zhang S, Du H, Fu Y. Fundamental principles and applications of microfluidic systems. *Front Biosci* 2008;13(7):2757–73.
- [31] Pamme N. Continuous flow separations in microfluidic devices. *Lab Chip* 2007;7(12):1644–59.
- [32] Lenshof A, Laurell T. Continuous separation of cells and particles in microfluidic systems. *Chem Soc Rev* 2010;39(3):1203–17.
- [33] Gossett DR, Weaver WM, Mach AJ, Hur SC, Tse HTK, Lee W, et al. Label-free cell separation and sorting in microfluidic systems. *Anal Bioanal Chem* 2010;397(8):3249–67.
- [34] Tsutsui H, Ho CM. Cell separation by non-inertial force fields in microfluidic systems. *Mech Res Commun* 2009;36(1):92–103.
- [35] Chaudhuri O, Cooper-White J, Janmey PA, Mooney DJ, Shenoy VB. Effects of extracellular matrix viscoelasticity on cellular behaviour. *Nature* 2020;584(7822):535–46.
- [36] Hu J, Jafari S, Han Y, Grodzinsky AJ, Cai S, Guo M. Size- and speed-dependent mechanical behavior in living mammalian cytoplasm. *Proc Natl Acad Sci USA* 2017;114(36):9529–34.
- [37] Moeendarbary E, Valon L, Fritzsche M, Harris AR, Moulding DA, Thrasher AJ, et al. The cytoplasm of living cells behaves as a poroelastic material. *Nat Mater* 2013;12(3):253–61.
- [38] Schuergers N, Nürnberg DJ, Wallner T, Mullineaux CW, Wilde A. PiB localization correlates with the direction of twitching motility in the cyanobacterium *Synechocystis* sp. PCC 6803. *Microbiology* 2015;161:960–6.
- [39] Bachin D, Nazarenko LV, Mironov KS, Pisareva T, Allakhverdiev SI, Los DA. Mechanosensitive ion channel MscL controls ionic fluxes during cold and heat stress in *Synechocystis*. *FEMS Microbiol Lett* 2015;362(12):fnnv090.
- [40] Haswell ES, Phillips R, Rees DC. Mechanosensitive channels: what can they do and how do they do it? *Structure* 2011;19(10):1356–69.
- [41] Perozo E, Cortes DM, Sompornpisut P, Kloda A, Martinac B. Open channel structure of MscL and the gating mechanism of mechanosensitive channels. *Nature* 2002;418(6901):942–8.